ACS APPLIED MATERIALS & INTERFACES

www.acsami.org
Research Article

A Nanoplasmonic Assay for Point-of-Care Detection of Mannose-Binding Lectin in Human Serum

Alessia Pancaro, Michal Szymonik, Patricia Perez Schmidt, Gizem Erol, Africa Garcia Barrientos, Laura Polito, Marco Gobbi, Sam Duwé, Jelle Hendrix, and Inge Nelissen*

Cite This: ACS Appl. Mater. Interfaces 2024, 16, 30556−30566

ABSTRACT: Mannose-binding lectin (MBL) activates the complement system lectin pathway and subsequent inflammatory mechanisms. The incidence and outcome of many human diseases, such as brain ischemia and infections, are associated with and influenced by the activity and serum concentrations of MBL in body fluids. To quantify MBL levels, tests based on ELISA are used, requiring several incubation and washing steps and lengthy turnaround times. Here, we aimed to develop a nanoplasmonic assay for direct MBL detection in human serum at the point of care. Our assay is based on gold nanorods (GNRs) functionalized with mannose (Man-GNRs) *via* an amphiphilic linker. We experimentally determined the effective amount of sugar linked to the nanorods' surface, resulting in an approximate grafting density of 4 molecules per nm^2, and an average number of 11 to 13 MBL molecules binding to a single nanoparticle. The optimal Man-GNRs concentration to achieve the highest sensitivity in MBL detection was 15 $\mu g \cdot mL^{-1}$. The specificity of the assay for MBL detection both in simple buffer and in complex pooled human sera was confirmed. Our label-free biosensor is able to detect MBL concentrations as low as 160 $ng \cdot mL^{-1}$ within 15 min directly in human serum *via* a one-step reaction and by using a microplate reader. Hence, it forms the basis for a fast, noninvasive, point-of-care assay for diagnostic indications and monitoring of disease and therapy.

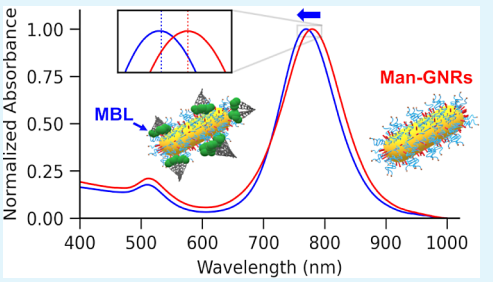

KEYWORDS: *mannose-binding lectin, gold nanorods, mannose surface functionalization, localized surface plasmon resonance, label-free biosensor*

INTRODUCTION

Mannose-binding lectin (MBL) is a collagen-like serum protein and a major component of the innate immune system, which is classified as an acute-phase protein because its blood levels increase after the onset of inflammation. The main function of MBL is the activation of the complement system lectin pathway and the subsequent inflammatory mechanisms. This is driven by the recognition and binding of specific carbohydrate motifs, such as mannose and *N*-acetylglucosamine, which are frequently present on a wide range of microbial surfaces (pathogen-associated molecular patterns, PAMPs) or are expressed by damaged host cells (damage-associated molecular patterns, DAMPs).[1,2] MBL activates the complement cascade that leads to opsonization, phagocytosis, and lysis of target microorganisms, thus playing a protective role.[3] In infections caused by severe acute respiratory syndrome coronavirus (SARS-CoV), MBL has previously been shown to bind the SARS-CoV spike protein, including that of SARS-CoV-2 variants of concern that caused the recent COVID-19 pandemic.[4,5] Stravalaci *et al.* showed that MBL recognizes the SARS-CoV-2 spike protein in a glycan-dependent manner and has antiviral activity in three *in vitro* models.[6] In the context of sterile inflammation, the activation of complement may induce several effects, such as expression of adhesion molecules, activation of leukocytes, and secretion of cytokines and chemokines, that could result in extensive tissue damage, detrimental for the host.[3,7] The incidence and outcome of many human diseases that are characterized by an acute inflammatory phase, such as rheumatoid arthritis,[8] diabetic nephropathy,[9] inflammatory bowel disease,[10] and cerebral ischemia,[11,12] are associated with and influenced by the activity and serum concentrations of MBL in body fluids.

Healthy adult Caucasian individuals generally have MBL levels above 1 $\mu g \cdot mL^{-1}$,[13] but during inflammation, MBL levels increase 3 to 4-fold compared to the baseline level.[14] The allelic variants and frequency variation among ethnic groups alter MBL transcription and translation, prevent oligomerization of MBL subunits, or significantly up- or down-regulate MBL expression, directly affecting the plasma level.[15] On the other hand, MBL deficiency, determined mainly by genetics, is defined in adults as a plasmatic concentration lower than 0.5

Received: March 11, 2024
Revised: May 2, 2024
Accepted: May 8, 2024
Published: May 28, 2024

https://doi.org/10.1021/acsami.4c04018
ACS Appl. Mater. Interfaces 2024, 16, 30556−30566

$\mu g \cdot mL^{-1}$[16] and is associated with a higher risk, severity, and frequency of infections,[17,18] as well as worse outcomes during severe systemic infections, such as sepsis.[19] For determining MBL deficiency caused by variability in the *MBL2* gene, an assay based on a mini-sequencing method for combined detection of six single-nucleotide polymorphisms was developed and used for the haplogenotyping of healthy individuals from the Czech population, but the isolation and quality of the DNA are the main limitations for its use outside of the laboratory.[20]

Monitoring of MBL levels may offer the opportunity of detecting disease-based increases or pathogenic decreases, and evaluation of the disease course.[21] MBL serum levels are typically measured by using enzyme-linked immunosorbent assays (ELISAs). These require either a significant hands-on time for manual execution or specialized, expensive, and high-maintenance equipment to enable the automated execution of the assay. Moreover, requirement of multiple supporting reagents and the multistep nature of ELISA are the main limitations for its use as a point-of-care test.[22] A rapid, simple MBL assay capable of being adopted in a point-of-care setting would be beneficial for a number of diagnostic and therapeutic applications.

In the current study, we aimed to develop an alternative MBL detection assay for direct measurement in biological fluids, comprising a fast, one-step, and wash-free process requiring minimal sample processing.

Our assay is based on the localized surface plasmon resonance (LSPR) phenomenon of gold nanorods (GNRs). The longitudinal plasmon band of GNRs is highly sensitive to local refractive index changes of the surrounding medium.[23] *Via* a careful choice of the rod geometry, this band can lie in the near-infrared region, where biological fluids exhibit the highest optical transparency.[24,25] Binding of biomolecules to the gold nanorods' surface leads to changes in the spectral properties of the LSPR peak, which has been exploited to produce biosensor devices for rapid, simple, label-free, and sensitive detection of low target molecule concentrations.[26]

Lectins typically exhibit only weak affinity toward simple monosaccharides. Multivalent presentation of such sugars on the surface of nanoparticles leads to a nonlinear increase in the binding affinity. This "cluster glycoside effect" has been exploited to produce high-affinity lectin-binding systems.[27] Glycosylated polymer-coated gold nanospheres have been applied by Gibson and coworkers for the sensitive, label-free detection of lectins in lateral flow and flow-through,[28,29] and glycosylated polymer-coated gold nanorods for binding the SARS-CoV-2 spike protein showing correlation to the presence of SARS-CoV-2 in primary COVID-19 clinical samples.[30] For high-affinity MBL recognition and binding, we developed so-called Man-$EG_6C_{11}S$-coated GNRs, consisting of monovalent mannose coupled onto the GNR surfaces using an amphiphilic linker (EG_6C_{11}−SH) containing six units of ethylene glycol. Similarly Man-$EG_6C_{11}S$-coated gold nanospheres have recently shown promising results as MBL inhibitors using an SPR-based assay.[31] The highly flexible chain of polyethylene glycol (PEG) can adopt a wide variety of conformations making undesired interactions with proteins or other blood components under physiological conditions thermodynamically unfavorable.[32] Moreover, due to the hydrophilic nature of the ethylene glycol chain, it generates a hydrated cloud leading to a low attraction of surrounding proteins.[33] Glyco-PEG coating of spherical gold nanoparticles and gold nanorods not only ensures high colloidal stability and biocompatibility, but also preserves the lectin binding in protein-rich biological media.[34] These properties make them ideal for the development of a label-free *in vitro* diagnostic assay. Furthermore, lactose-functionalized GNRs demonstrated good specificity to the cancer biomarker galectin-1 in aqueous solutions or in complex and heterogeneous serum specimens.[35]

In developing glyco-nanoparticles for therapeutic and diagnostic use, the density of the particle coating and the surrounding medium are key for glyco-NP interactions with target lectins. Here, we have investigated these aspects, as well as the mannose-coated GNR dose and the sensitivity and specificity of MBL detection, providing a solid proof of concept for a label-free nanoplasmonic assay.

MATERIALS AND METHODS

Reagents. Citrate-stabilized gold nanorods (GNRs) of 10 nm width and 38 nm length (λ_{max} = 780 nm) were purchased from Nanopartz (Loveland, USA) (3.8 $mg \cdot mL^{-1}$). D-(+)-Mannose, NaCl, trifluoroacetic acid, sulfuric acid (98% w/v), anthrone, and mannan-agarose beads were all purchased from Merck (St. Louis, USA); veronal buffer from Lonza Bioscience (Basel, Switzerland); pooled human serum (off-the-clot, type AB, male, sterile filtered) from Pan-biotech (Aidenbach, Germany); recombinant human MBL protein (rhMBL) (9086-MB), human MBL antibody (MAB2307) and Human MBL Quantikine ELISA from R&D Systems (Minneapolis, Canada). The thiol-linker $COOH-OCH_2-(O-CH_2-CH_2)_6(CH_2)_{11}SH$ (termed $COOH-OCH_2-EG_6C_{11}SH$ where $(O-CH_2-CH_2)_6$ = EG_6 and $(CH_2)_{11}$ = C_{11}) was purchased from Prochimia (Gdynia, Poland). Gibco Dulbecco's phosphate buffered saline (DPBS) with calcium and magnesium and EZ-Link NHS-PEG4-biotin were purchased from Fisher Scientific (Massachusetts, USA).

Synthetic mannose and glucose derivatives, termed Man-$EG_6C_{11}SH$ and Glc-$EG_6C_{11}SH$ respectively, were prepared as described previously[36] by Midatech Pharma (Bilbao, Spain) and dissolved in water.

All reagents used for the confocal microscope were purchased from Fisher Scientific, while precision cover glasses (22 × 22 × 0.17 mm) and microscope slides (26 × 76 × 1 mm) were purchased from Thorlabs (New Jersey, USA).

The preparation of the GNRs was conducted using Milli-Q grade water (resistivity of 18.2 mΩ·cm at 25 °C, 4 ppb total organic carbon). Eppendorf Protein LoBind tubes were used for all experiments involving rhMBL or human serum.

(Glyco)ligand Conjugation onto Gold Nanorod Surface. Citrate-stabilized gold nanorods were functionalized with thio-(glyco)ligands (*i.e.*, Man-$EG_6C_{11}SH$, Glc-$EG_6C_{11}SH$, and $COOH-OCH_2-EG_6C_{11}SH$). Briefly, 700 μL of GNRs suspension in water (2 $mg \cdot mL^{-1}$) was added dropwise to 15 μL of thio-(glyco)ligands solution (2 or 100 $mg \cdot mL^{-1}$) and incubated for 1 h at room temperature on a shaker (30 rpm) in the dark. The conjugates (termed Man-GNRs, Glc-GNRs, and COOH-GNRs, respectively) were sonicated for 1 min using a 40 kHz ultrasonic bath (Branson CPX1800H) and centrifuged at 12 000 g and 20 °C for 10 min, and the supernatant was removed. This was followed by 3 cycles of washing by resuspension in 1 mL of water, centrifugation, and removal of the supernatant by pipetting. A Sigma 3−30KS centrifuge was used with 1.5 mL volume tubes for all preparative centrifugations. The particles were finally resuspended in 0.5 mL of water and stored in polypropylene tubes at 4 °C until

https://doi.org/10.1021/acsami.4c04018
ACS Appl. Mater. Interfaces 2024, 16, 30556−30566

use. The GNRs suspensions were concentrated by centrifugation if needed.

MBL-Depleted Human Serum. MBL-depleted human serum was prepared according to a method described previously.[37] Briefly, a 5 mL column containing 2 mL of mannan-agarose as depleting beads was equilibrated with veronal buffer containing calcium chloride (3 mM) and magnesium chloride (10 mM). Human serum was passed through the column, and the flow-through was collected. The depletion of MBL was confirmed by Human MBL Quantikine ELISA (R&D Systems) showing ≥94% depletion efficiency (74 ± 4 ng·mL^{-1} of residual native MBL).

UV−Vis Spectroscopy. UV−Vis absorption spectra were acquired at 25 °C by using a CLARIOstar Plus spectrophotometer (BMG Labtech, Ortenberg, Germany). All absorbance spectra were recorded in the range of λ = 400−1000 nm with 1 nm resolution, in clear, flat-bottom 384-well plates (NUNC). The plates were shaken for 30 s at 100 rpm before each measurement. Results were smoothed using a Savitzky-Golay filter (order 4, window width 31), and full width at half-maximum (FWHM) and peak asymmetry (*i.e.*, a measure of peak tailing defined as the distance from the center line of the peak to the back slope divided by the distance from the center line of the peak to the front slope) were estimated. Peak maxima were determined from zero crossings of the derivative of the smoothed data. LSPR wavelength peak shift is expressed relative to the peak position at the start of the injection. All measurements were performed with at least three replicates ($n \geq 3$).

Functionalized GNRs (5 μL of a 240 μg·mL^{-1} suspension in water to reach a final concentration of 15 μg·mL^{-1}) were added to a series of different concentrations of rhMBL (0−2 μg·mL^{-1}) in 75 μL of DPBS. For the assay carried out in human serum, 5 μL of different concentrations of Man-GNRs were added to 75 μL of serum containing 1.2, 0.6, or 0.3 μg·mL^{-1} native MBL (nMBL) to reach a final Man-GNRs concentration of 3.5 μg·mL^{-1}, 7 μg·mL^{-1}, 15 μg·mL^{-1}, 30 μg·mL^{-1}, and 60 μg·mL^{-1}. The concentration of nMBL was confirmed using Human MBL Quantikine ELISA. Human serum containing 1.2 μg·mL^{-1} nMBL was 2-fold serially diluted in MBL-depleted human serum (preparation as described above) down to 0.11 μg·mL^{-1}. Absorbance spectra were recorded every 2.5 min after addition of 15 μg·mL^{-1} (final concentration) (glyco)ligand-coated GNRs. GraphPad Prism 9.5.1 software ordinary one-way ANOVA with Tukey's multiple comparison test was performed on nMBL binding data acquired at 15 min, and the ordinary 2-way ANOVA with Tukey's multiple comparison test was used to analyze time-dependent and nMBL concentration-dependent statistical differences.

ELISA. The 4.5 h solid phase assay (Human MBL Quantikine ELISA Kit (DMBL00) from R&D Systems) was performed according to the instructions provided by the manufacturer. Serum samples diluted 20 to 400-fold in a calibrator diluent (buffered protein solution with preservatives) were added in duplicates according to the manufacturer's guidelines. Eight human MBL standards (from 10 to 0.156 ng·mL^{-1} with 2-fold serial dilution and 0 ng·mL^{-1}) provided with the kit and reconstituted with calibrator diluent were assayed in parallel.

Ionic Strength Stability Studies. A solution of 1 M NaCl was 2-fold serially diluted down to 0.031 M in a 384-well plate. Citrate-GNRs and conjugated GNRs were added to each well to a final concentration of 15 μg·mL^{-1}, mixed, and incubated at room temperature for 30 min, and then an absorbance spectrum was recorded.

Nanoparticle Tracking Analysis (NTA). NTA was performed to measure GNRs' size before and after functionalization using a NanoSight NS500 instrument (NanoSight, Wiltshire, UK) in scatter mode with a laser output of 75 mW at 532 nm (green) and sCMOS camera (camera level set at 15). All samples were analyzed in water in duplicate at 25 °C, and 3 videos of 60 s were recorded (1499 frames with 25 frames/second) for each sample. The number of particles per frame ranged from 40 to 80 for the GNR samples, and none were detected in the buffer control. The samples were diluted to 10^8−10^9 particles·mL^{-1} in Milli-Q water prior to loading in the measurement chamber. For calibration, 100 nm polystyrene (PS) spheres were used. The mode was derived from a particle number concentration-based size distribution using NTA software version 3.0. For the analysis, a detection threshold of 4 was used.

ζ-Potential. The ζ-potential was measured on a ZetaView PMX-220 instrument (Particle Metrix, Inning am Ammersee, Germany). Zeta potential standard (Al_2O_3) was used for verification of the zeta potential. All samples were measured in 1 mM NaCl at 11 positions at 22 °C in triplicate (n = 3). Zeta potential was automatically calculated from the corresponding electrophoretic mobilities (μE) by using Henry's correction of the Smoluchowski equation. Software version 8.05.11 SP2 was used.

Differential Centrifugal Sedimentation (DCS). DCS was performed to assess GNRs functionalization by measuring the particles' size distribution. For this, a CPS DC24000 UHR disc centrifuge (Oosterhout, The Netherlands) was used with an 8−24% (w/w) sucrose gradient and a rotation speed of 24 000 rpm. Before each run, polyvinyl chloride latex beads (239 nm) with a particle density of 1.385 g·mL^{-1} were measured as a calibration standard. All measurements were performed with at least three replicates ($n \geq 3$). As the settling of particles is shape-dependent, for GNRs a "nonsphericity factor" (NSF) of 2.85 was applied in the CPS software. The concentration of particles at each size is determined by continuously measuring the turbidity of the fluid near the outside edge of the rotating disc. The disc centrifuge control system software automatically converts the turbidity measurements to a weight distribution using Mie Theory light scattering calculations and determines the particle diameter based on the settling time using the Stokes equation. The peak diameter was derived from particle weight-based size distribution plots.

Transmission Electron Microscopy (TEM). TEM micrographs were collected using a TEM-Zeiss LIBRA 200FE, equipped with 200 kV FEG, in-column second-generation omega filter for energy selective spectroscopy (EELS) and imaging (ESI), HAADF STEM facility, EDS probe for chemical analysis, and an integrated tomographic HW and SW system. The samples for TEM analysis were prepared by depositing a drop of nanoparticle solution on holey carbon copper grids (300 mesh) and evaporating the solvent. The particle size distribution was obtained by measuring at least 300 nanoparticles.

Anthrone−Sulfuric Acid Microplate Assay. This assay was used to determine the amount of mannose bonding on GNRs as previously described.[38] Briefly, the anthrone reagent was prepared right before analysis by dissolving 0.1 g of anthrone (0.1% w/v) in 100 mL of concentrated sulfuric acid

https://doi.org/10.1021/acsami.4c04018
ACS Appl. Mater. Interfaces 2024, 16, 30556−30566

(98% w/v) and protecting it from light. The anthrone solution was added slowly to the microplate containing various concentrations of D-mannose in water (4−125 $\mu g \cdot mL^{-1}$) to obtain a calibration curve, blank, Man-GNRs and COOH-GNRs at different concentrations (0.5, 0.8, and 1 $mg \cdot mL^{-1}$). The microplate was incubated for 10 min at 4 °C and then 20 min at 100 °C. After cooling to room temperature, the absorbance at 620 nm was measured, and the data were plotted against the concentration of D-mannose. The absorbance at 620 nm of the COOH-GNRs was used as the background deducted from the total signals measured from the Man-GNRs. All measurements were taken at least in duplicate ($n \geq 2$).

High-Performance Anion-Exchange Chromatography-Pulsed Amperometric Detection (HPAEC-PAD). HPAEC-PAD was used to analyze total saccharide concentration after acid hydrolysis to release mannose monosaccharides. Two concentrations of Man-GNRs and COOH-GNRs in water (0.5 and 2.25 $mg \cdot mL^{-1}$) and monovalent mannose sugar (160 $\mu g \cdot mL^{-1}$) as reference were hydrolyzed in 4 M trifluoroacetic acid for 2 h and 30 min at 100 °C. Man-GNRs and COOH-GNRs were washed twice in 200 μL of Milli-Q water *via* centrifugation (2000 g for 5 min) to remove nanoparticles. The supernatant was collected and dried under nitrogen overnight. The samples were redispersed in 400 μL of Milli-Q water and analyzed using a Dionex ICS-5000 (Thermo Scientific, Inc., Waltham, USA). The separation of monosaccharides was carried out with a Dionex CarboPac PA100 (4 mm × 250 mm) column coupled to a Dionex CarboPac PA100 (4 mm × 50 mm) guard column at a temperature of 25 °C, and an automated sample injector with an injection volume of 10 μL and a flush volume of 250 μL, as previously described.[39] All samples were diluted in Milli-Q water, and different standards (mannose, DP2-mannobiose, DP3-mannotriose, DP4-mannotetraose, DP5-mannopentaose, and DP6-mannohexaose) were used at concentrations from 5 to 150 $mg \cdot L^{-1}$. The resulting chromatographic data were processed using Chromeleon. Quantification was performed with a quadratic calibration curve.

Quantification of MBL Binding to Man-GNRs. A volume of 30 μL of Man-GNRs and COOH-GNRs prepared in water as described in "(glyco)ligand conjugation onto gold nanorod surface" was added to 1 mL of human serum containing 1.2 $\mu g \cdot mL^{-1}$ nMBL to reach different final concentrations (15 $\mu g \cdot mL^{-1}$; 30 $\mu g \cdot mL^{-1}$; 60 $\mu g \cdot mL^{-1}$; 80 $\mu g \cdot mL^{-1}$). They were prepared in duplicate and incubated at room temperature for 1 h on a shaker at 40 rpm to enable the formation of a biomolecule corona on the particles' surface. Moreover, 80 $\mu g \cdot mL^{-1}$ Man-GNRs were also prepared in MBL-depleted serum. The GNRs suspensions were centrifuged at 12 000*g* for 10 min at 4 °C, and the supernatant was collected, while the pellet was resuspended in 1 mL of DPBS. The samples were washed three times by pipetting in 1 mL of DPBS and redispersed in 35 μL of DPBS for SDS-PAGE and western blot densitometry analysis. The supernatant was collected after every centrifugation step and analyzed using a Human MBL Quantikine ELISA Kit.

Confocal Microscopy. Confocal microscopy was used to verify the binding between Man-GNRs and rhMBL in the buffer. rhMBL was first biotinylated using EZ-Link NHS-PEG4-biotin, and the excess biotin reagent removed using a Zeba spin desalting column, and then coupled to a streptavidin Alexa Fluor 647 conjugate (termed Alexa647-rhMBL). Man-GNRs, Glc-GNRs, and COOH-GNRs (15 $\mu g \cdot mL^{-1}$) with different concentrations of Alexa647-rhMBL in DPBS (0.125, 0.250, 0.5, and 1 $\mu g \cdot mL^{-1}$) were first incubated at room temperature for 1 h on a shaker at 40 rpm and then placed on cleaned microscope slides with a drop of ProLong gold antifade mountant and covered with coverslips. Prepared samples were protected from light and stored at room temperature for 24 h before the analysis. The same procedure was used for several controls.

Lasers at 633 and 543 nm were employed to visualize the fluorescence signal related to Alexa647-rhMBL and the light scattering signal of gold nanorods, respectively. FluoSpheres carboxylate-modified microspheres, 0.1 μm, yellow-green fluorescent (dilution 1:50000) were used to focus and adjust the lens. All images were recorded with a Zeiss LSM880 NLO AiryScan confocal microscope scan head mounted on the rear port of a Zeiss AxioObserver Z.1 inverted fluorescence microscope equipped with a Plan-Apochromat 63x/1.4 Oil DIC M27 oil immersion objective lens. More details are available in the Supporting Information. The microscope and acquisition configuration were controlled with the ZEN Black 2.6 SP1 software. Alignment of the Airyscan detector was performed by using the automated alignment procedure included in the control software. Airyscan processing was performed with the analysis package included in Zen Black. All images were processed by using the automatically determined processing strength. Five confocal images were analyzed for each set of experiments using CellProfiler software, and we calculated the number of nanoparticles and the correlation coefficient between Alexa647-rhMBL and GNRs.

RESULTS AND DISCUSSION

Gold Nanorods Functionalization and Stability. Citrate-stabilized GNRs were mixed with Man-$EG_6C_{11}SH$, Glc-$EG_6C_{11}SH$, or $COOH-OCH_2-EG_6C_{11}SH$ (100 $mg \cdot mL^{-1}$ each) to produce (glyco)ligand-coated GNRs (termed Man-GNRs, Glc-GNRs, and COOH-GNRs, respectively). The excess of ligands was removed by three centrifugation and resuspension cycles. The physicochemical properties of the resulting nanoparticles were characterized in Milli-Q water by UV−vis, DCS, ζ-potential, NTA, and TEM (Figure 1, Figure S1, and Table 1). UV−vis spectroscopy revealed a red shift of the longitudinal LSPR band for the glyco-coated GNRs, ζ-potential indicated a decrease of negative surface charge, and TEM showed that the nanorod dimensions were retained during coating, while DCS and NTA analyses indicated an increase in particle size compared with the citrate-GNRs, as expected (see Table 1). When nanoparticles are coated and therefore the resulting density and size are changed, their size measured by DCS is altered, showing here a shift toward apparent smaller diameters.[40,41] Altogether, these data confirmed the successful attachment of the glyco ligands to the particle surface and their stability in a colloidal suspension.

The high affinity of thiols for gold surfaces allows for the easy displacement of citrate ions from gold nanoparticle surfaces and produces a dense coverage of ligands.[42] The surface grafting density is a key parameter in stabilizing nanoparticles in suspension and producing an LSPR binding response to lectin interaction.[43] The monodispersity of gold nanoparticles is a crucial factor for diagnostic and therapeutic applications[44] and when applied as sensors, higher sensitivity can be achieved with a smaller FWHM.[45] Lack of symmetry and right-sided distortion of the longitudinal LSPR band of

https://doi.org/10.1021/acsami.4c04018
ACS Appl. Mater. Interfaces 2024, 16, 30556−30566

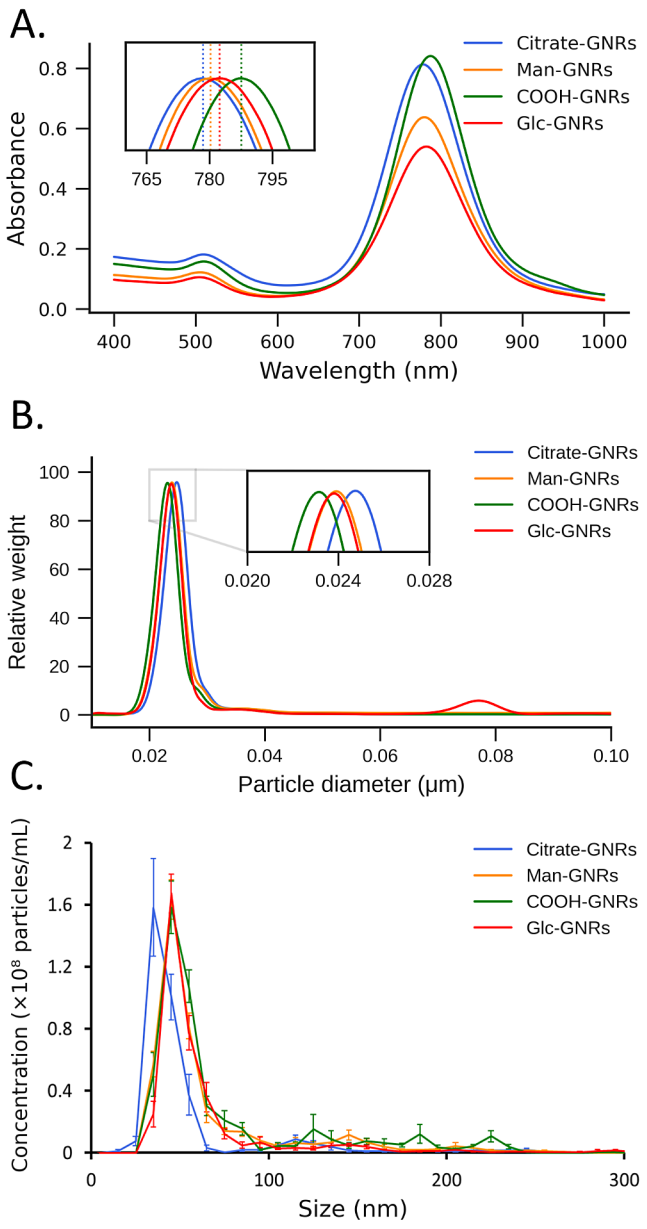

Figure 1. Characterization of citrate-GNRs, Man-GNRs, Glc-GNRs, and COOH-GNRs. (A) UV−vis absorption spectra (Inset: zoomed view on the LSPR peak bands after normalization to better visualize the LSPR shift). (B) Particle weight-size distribution plots obtained by DCS (Inset: zoomed view of the peaks of the size distribution). (C) Particle number concentration-size distribution plots obtained by NTA. A representative example of one out of three replicate measurements is shown.

gold nanorods are a sign of high polydispersity in size and aspect ratio or slight aggregation.

To analyze the impact of low *versus* high grafting densities on glyco-conjugated GNR stability, citrate-GNRs (700 μL, 2 mg·mL^{-1}) were functionalized with 15 μL of 2 mg·mL^{-1} or 100 mg·mL^{-1} Man-$EG_6C_{11}SH$, respectively. Whereas 100 mg·mL^{-1} Man-$EG_6C_{11}SH$ resulted in equally stable Man-GNRs suspensions in both water and DPBS, the low grafting concentration of 2 mg·mL^{-1} (termed Man_{low}-GNRs) resulted in higher FWHM values and an increase in the peak asymmetry. This Man_{low}-GNRs instability was enhanced in DPBS compared to water as a dispersant as shown by the increase in the peak asymmetry (Table S1). The observations for Man_{low}-GNRs both in Milli-Q and in DPBS are further confirmed by a visible colorimetric shift in GNRs solutions from red to purple indicating nanoparticles' aggregation (Figure S2 and Table S1). Hence, the GNRs conjugation with 100 mg·mL^{-1} Man-$EG_6C_{11}SH$ was used for further assay development in this study. Moreover, the amphiphilic linker was also found to enhance the stability of the glyco-conjugated GNRs, as aggregation was observed by the naked eye when excess of Man-$C_{11}SH$ (without the EG moiety) was used.

Table 1. Characterisation of Glyco-Coated GNRs[a]

	UV−vis LSPR peak (nm)	ζ-potential (mV)	DCS peak diameter (nm)	NTA mode (nm)
citrate-GNRs	778 ± 1	- 45.2 ± 0.5	24.9 ± 0.1	40.6 ± 0.5
Man-GNRs	780 ± 1	- 37.8 ± 0.1	24.0 ± 0.1	46.0 ± 0.2
COOH-GNRs	787 ± 1	- 41 ± 1	23.3 ± 0.1	48.5 ± 0.6
Glc-GNRs	782 ± 1	- 37.5 ± 0.4	23.9 ± 0.2	46.8 ± 0.2

[a]UV-Vis LSPR peak (nm), ζ-potential (mV), peak diameter (nm) by DCS, and modal diameter (nm) by NTA of citrate-GNRs and (glyco)ligand-coated GNRs (N = 3, mean +/- SD).

The stability of the Man-GNRs suspensions was furthermore studied using a sodium chloride titration assay.[46] The colloidal stability of nanoparticles at physiological saline concentrations (~150 mM NaCl) is a prerequisite for any biomedical applications and a further indication of a successful functionalization. UV−vis spectroscopy analysis of the LSPR peak, which is highly sensitive to aggregation, showed aggregation of citrate-GNRs above 63 mM NaCl with the impossibility to analyze peak asymmetry and FWHM for concentration ≥125 mM NaCl. No significant changes have been observed in FWHM and peak asymmetry for all the functionalized GNRs that remained as stable dispersions up to 1 M NaCl (Figure S3). This improvement in stability confirms the suitability of the functionalized rods for testing in physiological salt levels minimizing the probability of false positives/negatives due to unwanted aggregation.

Man-GNRs Coating Density. To analyze the coating density of Man-GNRs, the amount of carbohydrate ligands coupled to gold nanorods *via* a thiol linker was determined by a colorimetry method using anthrone−sulfuric acid. This technique for the quantitative analysis of carbohydrates[38] has been previously adopted in glyconanoparticle analysis.[35] The amount of mannose attached to GNRs was subsequently derived from the calibration curve and estimated to be 5506 ± 885 mannose molecules per nanorod (calculated from 31 ± 5 μg·mL^{-1} (175 ± 28 μM) mannose in 1 mg·mL^{-1} (0.032 μM) Man-GNRs, Figure S4 and Table S2). The same method was employed in other two studies to measure the presence of lactose on GNRs: a concentration of 110 μg·mL^{-1} was determined on 2 mg·mL^{-1} Lac-GNRs;[35] a value of 5499 ± 428 lactose molecules per nanorod was estimated for Lac-EG_4C_{11} coated GNRs.[34] It is important to point out that in the latter study, compared to ours, the different geometries of GNRs used (64 × 16 nm *vs.* 38 × 10 nm), sugar (Lac *vs.* Man), and linker ($EG_4C_{11}SH$ *vs.* $EG_6C_{11}SH$), respectively, led to a different glyco organization on the GNR surface.

A noncolorimetric method, HPAEC-PAD, which enables separation of gold nanorods before the quantification, was also

https://doi.org/10.1021/acsami.4c04018
ACS Appl. Mater. Interfaces 2024, 16, 30556−30566

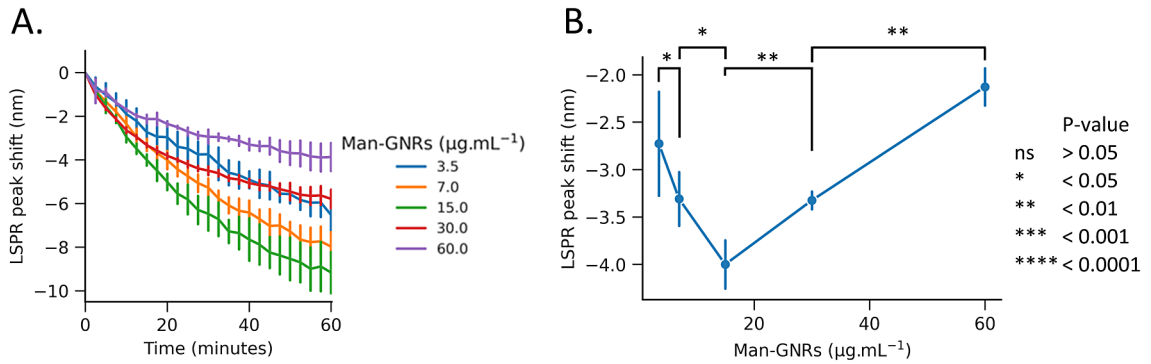

Figure 2. LSPR binding response of different concentrations of Man-GNRs to nMBL (1.2 $\mu g \cdot mL^{-1}$) in human serum. (A) The lines indicate the LSPR peak shift of Man-GNRs in serum as a function of time for different Man-GNRs concentrations. (B) LSPR wavelength peak shift after 15 min as a function of Man-GNRs concentration is expressed relative to the peak position at the start of the injection. All the measurements were performed with at least three replicates ($n \geq 3$, mean ± SD). One-way ANOVA with Tukey's multiple comparison test was used. *P*-value: ns >0.05; * < 0.05; ** < 0.01; *** < 0.001; **** < 0.0001.

applied to estimate the number of carbohydrates per nanoparticle. HPAEC-PAD enables sensitive detection for carbohydrate analysis and has been previously employed to quantify sugar linked to gold nanoparticles.[47] Man-GNRs and COOH-GNRs showed results close to the anthrone–sulfuric acid colorimetric assay: an interpolated concentration of 26.6 ± 0.4 $\mu g \cdot mL^{-1}$ (148 ± 3 μM) of mannose for 1 $mg \cdot mL^{-1}$ Man-GNRs (4660 ± 67 mannose molecules per nanorod) and no sugar detected for the COOH-GNRs control. Moreover, monovalent mannose sugar (160 $\mu g \cdot mL^{-1}$) treated and analyzed in the same way, was used as internal reference, leading to a concentration of 155 $\mu g \cdot mL^{-1}$ proving the reliability of the procedure.

Despite the HPAEC-PAD method determining the mannose concentration after the release from gold surface (as opposed to anthrone–sulfuric acid which directly quantify the mannose attached to gold), HPAEC-PAD is more reliable with a lower error due to the absence of gold absorbance interference. Both methods showed good agreement with the maximum theoretical number of thiol linkers able to bind the gold surface (5527 molecules). This is estimated considering the surface area of the GNRs used (1193.8 nm^2) and the structure of *n*-alkyl thiols on gold which has been studied and described as an hexagonal $\sqrt{3} \times \sqrt{3}R\ 30°$ arrangement of thiol molecules with a sulfur–sulfur distance of around 5 Å and an area per molecules of 21.6 $Å^2$.[48,49] Moreover, based on the HPAEC-PAD results, the mannose-PEG grafting density was calculated and found to be around 4 $molecules \cdot nm^{-2}$ (calculation in the Supporting Information). This is in agreement with the values reported in the literature in which for PEG ligands on spherical gold nanoparticles a grafting density of 3.5 $molecules \cdot nm^{-2}$ was obtained by quantitative proton nuclear magnetic resonance and thermogravimetric analysis,[50] and a surface coverage from 4.3 to 6.3 $molecules \cdot nm^{-2}$ by inductively coupled plasma mass spectrometry.[51]

Optimal Man-GNRs Concentration for MBL Binding Assay in Human Serum. In preliminary studies, we measured the LSPR binding response of Man-GNRs at a fixed GNRs concentration of 15 $\mu g \cdot mL^{-1}$ to varying concentrations of rhMBL in simple buffer, and observed aggregation with rhMBL concentrations above 0.5 $\mu g \cdot mL^{-1}$ (Figure S5 and Table S3). Control experiments indicated that the responses observed are due to specific carbohydrate–lectin interactions, as shown in Figure S6. Confocal microscopy studies also showed a high correlation between Man-GNRs and Alexa647-rhMBL in the buffer, which was not observed in the different controls used, confirming the specific binding (Figure S7). The binding response obtained in these first studies with rhMBL pointed out the need to further optimize the assay conditions to enable the measurement of physiological MBL concentrations (~1 $\mu g \cdot mL^{-1}$). However, the Man-GNRs behavior in simple buffer does not represent a clinical *in vitro* diagnostic scenario. In biofluids such as human serum, nanoparticles are exposed to many bio(macro)-molecules which adsorb to their surface, leading to the formation of a "biomolecular corona" which may influence the physicochemical properties and impact the binding properties of the nanoparticles.[52−54] For this reason, we decided to further evaluate the performance of Man-GNRs for the recognition of native MBL (nMBL) in the human serum complex environment.

Since the interaction between nMBL and Man-GNRs is dependent on the concentration of both species, we evaluated the rod concentration yielding the highest performance in terms of LSPR peak shift and reproducibility. Different Man-GNRs concentrations were added to undiluted pooled human serum which contained a natural concentration of 1.2 $\mu g \cdot mL^{-1}$ nMBL as determined by a commercially available Human MBL Quantikine ELISA Kit. The results showed statistically significant differences (*P*-value <0.05) between the different concentrations at 15 min read-out time (Figure 2B). The best performance was reached using a Man-GNRs concentration of 15 $\mu g \cdot mL^{-1}$, especially at early time points <20 min (Figure 2A,B).

The optimal Man-GNRs concentration was also evaluated in human serum containing lower concentrations of nMBL (0.64 $\mu g \cdot mL^{-1}$ and 0.36 $\mu g \cdot mL^{-1}$). The results are consistent with the behavior observed in Figure 2A and the same conclusions can be drawn with 15 $\mu g \cdot mL^{-1}$ of Man-GNRs reaching the best performance (Figure S8). In conclusion, we showed that the concentration of Man-GNRs strongly influences the biosensor performance. A constant rods concentration of 15 $\mu g \cdot mL^{-1}$ was used further in this study.

Assay Sensitivity and Specificity. Baseline MBL serum levels and function are genetically determined, but levels rise during infections and inflammation. An excess of MBL activation might lead to tissue damage due to an unbalanced inflammatory and coagulation response, whereas MBL

https://doi.org/10.1021/acsami.4c04018
ACS Appl. Mater. Interfaces 2024, 16, 30556−30566

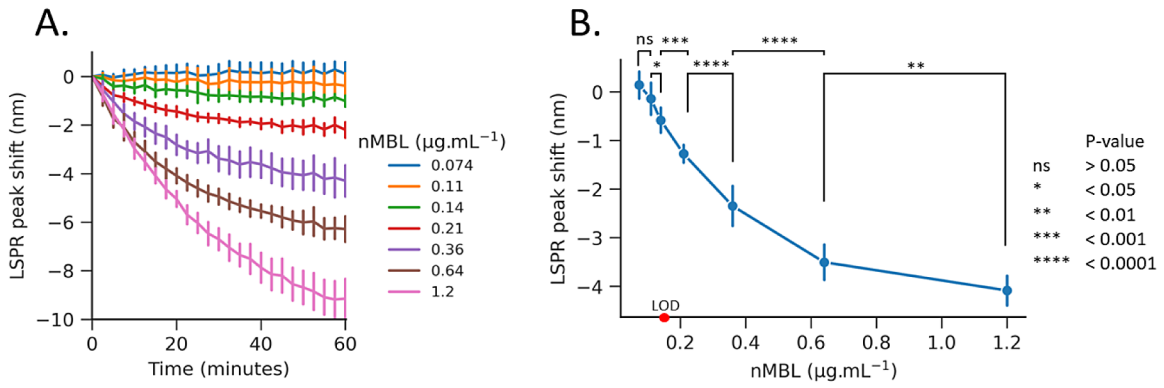

Figure 3. Determination of the LOD of the nMBL binding assay. (A) The lines indicate the LSPR peak shift of Man-GNRs (15 $\mu g \cdot mL^{-1}$) in human serum as a function of nMBL concentration over time. (B) LSPR wavelength peak shift with increasing nMBL concentration after 15 min, relative to the peak position at the start of the injection ($N = 4$, mean ± SD). LOD (0.16 $\mu g \cdot mL^{-1}$) is determined from the average and three times the standard deviation of blank measurements in a dose−response curve. One-way ANOVA with Tukey's multiple comparison test was used. *P*-value: ns >0.05; * < 0.05; ** < 0.01; *** < 0.001; **** < 0.0001.

deficiency confers a high risk for severe infections[55] and can predispose patients to SARS-CoV-2 infection.[56]

Using the optimized Man-GNRs concentration, we next evaluated the limit of detection (LOD) of nMBL in serum. For this, undiluted human serum containing 1.2 $\mu g \cdot mL^{-1}$ nMBL was 2-fold serially diluted down to 0.11 $\mu g \cdot mL^{-1}$ using MBL-depleted serum[57] to keep other serum constituents at physiological levels. Serum nMBL levels and the successful removal of nMBL from the same pooled serum batch (≥94% depletion efficiency) were measured with ELISA. A residual nMBL value of 0.074 ± 0.004 $\mu g \cdot mL^{-1}$ was found in MBL-depleted serum and was included in the dilution.

We monitored the LSPR peak over time following the addition of Man-GNRs using a microplate reader. Man-GNRs showed dose-dependent LSPR blue-shifts in serum (Figure 3A), typical indicative of the loss of material from the surface, as shown in a previous study where addition of a plant lectin led to binding and displacement of biocorona components due to specific lectin/glycan interactions.[58] Two-way ANOVA showed statistically significant time-dependent differences for concentrations above 0.14 $\mu g \cdot mL^{-1}$ (see Table S4).

Adult individuals generally present MBL levels close to 1 $\mu g \cdot mL^{-1}$ in healthy Caucasians with increased and lower levels associated with several conditions. We showed that our assay can measure nMBL directly in undiluted human serum. It is important to point out that a concentration of 1.2 $\mu g \cdot mL^{-1}$ nMBL was used as the highest point, because it was naturally present in the used pooled human serum. Higher concentrations require minimal sample dilution (*i.e.*, 2 to 4-fold considering that during inflammation, MBL levels increase 3 to 4-fold compared to the baseline level). This assay may directly measure concentrations >1.2 $\mu g \cdot mL^{-1}$, but a plateau is almost reached at 1.2 $\mu g \cdot mL^{-1}$ after 60 min. While ELISA is able to detect MBL concentrations much lower than our assay (e.g., R&D Systems, DMBL00, 0.2 $ng \cdot mL^{-1}$), for clinical use our assay can identify MBL-deficiency (*i.e.*, concentration <0.5 $\mu g \cdot mL^{-1}$) without any dilution required. Moreover, sequencing technologies[20] can be used as a complementary tool to confirm that severe pathogenic low MBL (<0.1 $\mu g \cdot mL^{-1}$) is caused by genetics. To obtain an assay capable of rapid measurement within the clinically relevant concentration range, we identified an incubation time of 15 min as the earliest time point for differential analysis (Figure 3B), while ELISAs require long turn-around time (3−4.5 h). One-way ANOVA identified statistically relevant differences (*P*-value <0.001) in the LSPR peak shift above 0.14 $\mu g \cdot mL^{-1}$ at 15 min read-out time, as shown in Figure 3B. Therefore, this assay has the potential to both identify MBL deficiencies and disease-related elevated levels. At 15 min read-out time and up to 1 h the LOD for native MBL detection in human serum using mannose-coated GNRs, determined from the average and three times the standard deviation of blank measurements in a dose−response curve, was found to be 0.16 $\mu g \cdot mL^{-1}$. LOD was also determined for different time points based on the standard deviation of the response and the slope of the calibration curve, excluding the two highest nMBL concentrations (0.64 and 1.2 $\mu g \cdot mL^{-1}$) to have a linear range. Using this approach, after 15 min as an acceptable assay response time, the LOD was 0.072 $\mu g \cdot mL^{-1}$, whereas the lowest LOD was found at 30 min (0.029 $\mu g \cdot mL^{-1}$).

The response of Man-GNRs to nMBL in serum was found to be reproducible across four different coupling reactions from 2 batches of GNRs ($N = 4$, Figure 3). An LSPR shift of 0.14 ± 0.28 was observed in MBL-depleted serum (containing 0.074 ± 0.004 $\mu g \cdot mL^{-1}$ of residual nMBL). In control experiments, using COOH-GNRs without glycan modification in human serum containing different nMBL concentrations (Figure S9A), or addition of Man-GNRs to different SBA concentrations in MBL-depleted serum, did not lead to any response (Figure S9B), confirming the selective nMBL recognition in complex media. To further assess the nMBL assay specificity, Glc-GNRs (15 $\mu g \cdot mL^{-1}$) were supplemented with the same nMBL dose series in serum. Glc-GNRs aggregated showing a high LSPR peak shift of ∼10 nm in just 15 min, which was independent of the nMBL dose (Figure S9C). This behavior could be explained by the binding of many proteins with affinity for glucose,[59] such as[60] human serum albumin, the most abundant serum protein. Besides confirming Man-GNRs' specificity, these experiments provided proof that the serum MBL-depletion strategy did not significantly affect other serum lectins, which have no affinity for mannose.

Finally, whereas the original nMBL assay was performed in a 384-well plate format, we have also verified and confirmed a similar assay performance in the commonly used 96-well format using a larger working volume (200 *vs.* 80 μL) (Figure S10).

https://doi.org/10.1021/acsami.4c04018
ACS Appl. Mater. Interfaces 2024, 16, 30556−30566

Quantification of MBL Binding to Man-GNRs. The behavior of nanoparticles in physiological systems is a highly dynamic process influenced by the nanoparticles' properties.[61] When added to human serum, Man-GNRs will not only bind the available nMBL with high affinity, but also form a surface-adsorbed corona of other serum biomolecules, mainly proteins. This biomolecular corona is formed through competitive interactions, also involving nMBL, and evolves over time, forming an inner layer of tightly bound molecules with a longer lifetime (termed "hard" corona), and an outer layer of weakly bound molecules with a shorter lifetime (called "soft" corona). We used here theoretical and experimental approaches to confirm the specificity of the interaction of Man-GNRs with nMBL and estimate the amount of lectin bound to every nanoparticle. Considering the surface area of one rod in relation to the area of the carbohydrate recognition domains of the MBL monomer (estimated *via* Pymol based on the protein structure PDB ID: 1HUP), the maximum amount of lectin molecules was estimated to be about 25, without considering intermolecular forces. The reliability of this value was experimentally tested by using ELISA and western blot densitometry.

A method commonly used for determining the amount of binding protein on the surface of nanoparticles is to measure the protein remaining in the supernatant after interaction.[62] We used ELISA to determine the concentration of unbound nMBL in the collected supernatant after incubation of several Man-GNRs and COOH-GNRs concentrations (15, 30, 60, and 80 $\mu g \cdot mL^{-1}$) in duplicate in human serum containing 1.2 $\mu g \cdot mL^{-1}$ nMBL, centrifugation, and washing steps. The amounts of nMBL bound to rods are listed in Table 2. For all COOH-GNRs concentrations, the level of bound MBL was below 60 $ng \cdot mL^{-1}$ (data not shown). Using these results, an average number of 11 to 13 nMBL monomers (formed by three identical polypeptide chains) binding onto each functionalized nanorod could be derived (calculations and Figure S11).

Table 2. Amount of nMBL Bound to Man-GNRs in Human Serum, Determined by ELISA and Western Blot (WB) Densitometry Analysis[a]

man-GNRs ($\mu g \cdot mL^{-1}$)	bound nMBL concentration ($ng \cdot mL^{-1}$ and %) by ELISA	bound nMBL concentration ($ng \cdot mL^{-1}$ and %) by WB
15	210 ± 30 (18%)	227 ± 6 (19%)
30	430 ± 40 (36%)	370 ± 20 (31%)
60	810 ± 20 (68%)	740 ± 40 (61%)
80	955 ± 34 (80%)	890 ± 20 (74%)

[a]Man-GNRs samples were prepared twice ($N = 2$) and a duplicate analysis ($n = 2$) was performed for each sample (mean ± SD). MBL bound (%) according to ELISA and WB compared to the start concentration of nMBL in human serum (1.2 $\mu g \cdot mL$-1).

Starting from the same Man-GNRs and COOH-GNRs incubations in serum, the concentration of effectively bound nMBL was also estimated using western blot (see the Materials and Methods section in the Supporting Information) followed by densitometry analysis. For this, the nanoparticle−corona complexes were isolated by a total of three centrifugation steps, resuspended in DPBS, and the pellet after every centrifugation step was characterized by SDS-PAGE and western blot (see the Materials and Methods in the Supporting Information). The abundance of GNRs' surface-adhered proteins making up the soft corona gradually decreased after the first three washes (Figure S12A). It has been demonstrated that the hard corona proteins do not elute from the NP surface after any additional washing steps.[63] The presence of nMBL bound on the Man-GNRs' surface was confirmed by western blot (Figure S12B) after every washing step (as expected), with the decreasing amount indicating an appearance in both the soft and hard corona. No traces of the lectin were observed in the control COOH-GNRs samples, as well as for Man-GNRs incubated in MBL-depleted serum (Figure S12C). Moreover, the concentration of nMBL present in the hard corona was estimated in a second western blot loaded with different sample dilutions using densitometry analysis against a known amount of rhMBL (Figure S12D). The derived concentrations were in good agreement with the ELISA results, as shown in Table 2. The higher amount observed for the ELISA values can be explained considering that the amount of nMBL is measured in the supernatant containing unbound nMBL and washed off soft corona molecules, while with western blot only the hard corona after 3 washing steps is analyzed.

It is well-known that the function of MBL strongly depends on its oligomeric structure with large oligomers (mainly trimers and tetramers) activating the complement cascade through the lectin pathway, while monomers and small oligomers act as opsonins.[64] The theoretical maximum amount estimated to be about 25 is based on monomers whereas in blood there is a variety of MBL oligomeric forms which have a direct effect on carbohydrate-binding properties.[65] Moreover, the MBL pattern recognition molecule circulates in blood in complexes with MBL-associated serine proteases (MASPs).[66] SDS-PAGE and western blot confirm the presence of molecules bound to MBL (Figure S12A,B) since higher molecular weight complexes can be detected under reducing conditions with the polypeptide chain of MBL having an apparent mass of ∼32 kDa. To further prove the presence of proteins bound to MBL, we purified nMBL from pooled human serum using column chromatography and analyzed by liquid chromatography−mass spectrometry (LC-MS) (see the Methods section in the Supporting Information). Besides MASPs, we found several protein components with a percentage >1%, of which serum amyloid p-component, alpha-2-macroglobulin, and immunoglobulin (Table S5) have previously been reported to interact with MBL.[67−69] The presence of trypsin can be caused by sample handling. Therefore, oligomers impose a larger intermolecular distance explaining the lower experimental values of 11 to 13 nMBL monomers compared to the theoretical value of 25.

CONCLUSIONS

We report here on a new nanoplasmonic biosensing platform for MBL detection in human serum, which we developed toward a point-of-care MBL assay faster and simpler than standard ELISA to be employed in several scenarios and in large patient cohorts. Man-GNRs biosensors were designed and fabricated for the detection of MBL based on the high affinity for mannose and unique LSPR properties of GNRs.

The core of our assay consists of Man-GNRs conjugates showing an approximate mannose-PEG grafting density of 4 molecules per nm^2 and 4660 mannose molecules per particle. We confirmed the interaction of Man-GNRs with nMBL in human serum and determined the amount of lectin bound to every nanoparticle to be 11 to 13. The assay specificity for nMBL in complex serum environment was demonstrated, with a limit of detection as low as 160 $ng \cdot mL^{-1}$ in just 15 min by

https://doi.org/10.1021/acsami.4c04018
ACS Appl. Mater. Interfaces 2024, 16, 30556−30566

using a microplate reader, enabling the measurement of MBL concentrations within the physiological and pathological range directly from complex biofluids.

This proof-of-concept for a fast, easy to perform, single-step assay using only a microplate reader shows major promise for adaptation into a rapid point-of-care diagnostic.

■ ASSOCIATED CONTENT

Supporting Information

The Supporting Information is available free of charge at https://pubs.acs.org/doi/10.1021/acsami.4c04018.

Confocal microscopy, TEM images, UV−vis spectroscopy analysis of Man_{low}-GNR stability, salt titration assay, anthrone/sulfuric acid assay-calibration curve, calculation of D-mannose density on GNRs, recombinant human MBL detection in buffer and human serum, confocal microscopy analysis, optimal Man-GNRs concentrations for MBL binding assay in human serum, two-way ANOVA, native MBL detection controls in human serum, MBL binding assay performed in 96-well format, calculation of number of nMBL molecules binding one rod, SDS-PAGE and western blotting, purified nMBL and liquid chromatography−mass spectrometry (PDF)

■ AUTHOR INFORMATION

Corresponding Author

Inge Nelissen − *Health Unit, Flemish Institute for Technological Research (VITO), Mol 2400, Belgium*; Email: inge.nelissen@vito.be

Authors

Alessia Pancaro − *Health Unit, Flemish Institute for Technological Research (VITO), Mol 2400, Belgium; Dynamic Bioimaging Lab, Biomedical Research Institute, Hasselt University, Diepenbeek 3590, Belgium*; orcid.org/0000-0003-4586-3531

Michal Szymonik − *Health Unit, Flemish Institute for Technological Research (VITO), Mol 2400, Belgium*

Patricia Perez Schmidt − *Istituto di Scienze e Tecnologie Chimiche "Giulio Natta", SCITEC−CNR, G, Milan 20138, Italy*

Gizem Erol − *Istituto di Ricerche Farmacologiche Mario Negri IRCCS, 20156 Milan, Italy*

Africa Garcia Barrientos − *Midatech Pharma PLC, Cardiff CF24 0AA, U.K.*

Laura Polito − *Istituto di Scienze e Tecnologie Chimiche "Giulio Natta", SCITEC−CNR, G, Milan 20138, Italy*; orcid.org/0000-0002-7756-2365

Marco Gobbi − *Istituto di Ricerche Farmacologiche Mario Negri IRCCS, 20156 Milan, Italy*; orcid.org/0000-0003-1014-6225

Sam Duwé − *Advanced Optical Microscopy Centre, Biomedical Research Institute, Hasselt University, Diepenbeek 3590, Belgium*; orcid.org/0000-0003-3768-1877

Jelle Hendrix − *Dynamic Bioimaging Lab, Biomedical Research Institute, Hasselt University, Diepenbeek 3590, Belgium; Advanced Optical Microscopy Centre, Biomedical Research Institute, Hasselt University, Diepenbeek 3590, Belgium*; orcid.org/0000-0001-5731-1297

Complete contact information is available at: https://pubs.acs.org/10.1021/acsami.4c04018

Author Contributions

The manuscript was written through contributions of all authors. All authors have given approval to the final version of the manuscript.

Notes

The authors declare the following competing financial interest(s): A.P., M.S. and I.N. have filed a patent application (EP22209662.0) based on this work in the name of VITO NV. The remaining authors declare no competing interests.

■ ACKNOWLEDGMENTS

This project received funding from the European Commission under grant N° 814236 of the Marie Curie European Training Network (MC-ETN) NanoCarb. This work is furthermore supported by VITO as well as by Hasselt University. We thank: Dr. Kathy Elst and Peter De Rechter (VITO) for HPAEC-PAD analysis; Dr. Stefano Fumagalli (Istituto di Ricerche Farmacologiche Mario Negri IRCCS) for useful discussions and comments on the manuscript; Prof. Dr. Geert Baggerman, Karin Schildermans and Dr. Jusal Quanico (VITO) for useful discussions and LC-MS analysis; Luigi Musetta (KU Leuven) for statistical data analysis. The used confocal microscope was funded *via* the Research Foundation Flanders (FWO, project G0H3716N). S.D. acknowledges the BOF-Methusalem (R-12960).

■ REFERENCES

(1) Ricklin, D.; Hajishengallis, G.; Yang, K.; Lambris, J. D. Complement: A Key System for Immune Surveillance and Homeostasis. *Nat. Immunol.* **2010**, *11* (9), 785−797.

(2) Takahashi, K.; Ip, W.; Michelow, I.; Ezekowitz, R. The Mannose-Binding Lectin: A Prototypic Pattern Recognition Molecule. *Curr. Opin. Immunol.* **2006**, *18* (1), 16−23.

(3) Kalia, N.; Singh, J.; Kaur, M. The Ambiguous Role of Mannose-Binding Lectin (MBL) in Human Immunity. *Open Med.* **2021**, *16* (1), 299−310.

(4) Wu, F.; Zhao, S.; Yu, B.; Chen, Y.; Wang, W.; Song, Z.; Hu, Y.; Tao, Z.; Tian, J.; Pei, Y.; et al. A New Coronavirus Associated with Human Respiratory Disease in China. *Nature* **2020**, *579* (7798), 265−269.

(5) Zhu, N.; Zhang, D.; Wang, W.; Li, X.; Yang, B.; Song, J.; Zhao, X.; Huang, B.; Shi, W.; Lu, R.; Niu, P.; Zhan, F.; Ma, X.; Wang, D.; Xu, W.; Wu, G.; Gao, G.; Tan, W. China Novel Coronavirus Investigating and Research Team A Novel Coronavirus from Patients with Pneumonia in China, 2019. *N. Engl. J. Med.* **2020**, *382* (8), 727−733.

(6) Stravalaci, M.; Pagani, I.; Paraboschi, E. M.; Pedotti, M.; Doni, A.; Scavello, F.; Mapelli, S. N.; Sironi, M.; Perucchini, C.; Varani, L.; et al. Recognition and Inhibition of SARS-CoV-2 by Humoral Innate Immunity Pattern Recognition Molecules. *Nat. Immunol.* **2022**, *23* (2), 275−286.

(7) Jacobson, S.; Larsson, P.; Åberg, A. M.; Johansson, G.; Winsö, O.; Söderberg, S. Levels of Mannose-Binding Lectin (MBL) Associates with Sepsis-Related in-Hospital Mortality in Women. *J. Inflamm.* **2020**, *17* (1), 28.

(8) Xu, J.; Chen, G.; Yan, Z.; Qiu, M.; Tong, W.; Zhang, X.; Zhang, L.; Zhu, Y.; Liu, K. Effect of Mannose-Binding Lectin Gene Polymorphisms on the Risk of Rheumatoid Arthritis: Evidence from a Meta-Analysis. *Int. J. Rheum. Dis.* **2021**, *24* (3), 300−313.

(9) Cai, K.; Ma, Y.; Wang, J.; Nie, W.; Guo, J.; Zhang, M.; Yang, Y.; Chen, J.; Han, F. Mannose-Binding Lectin Activation Is Associated with the Progression of Diabetic Nephropathy in Type 2 Diabetes Mellitus Patients. *Ann. Transl. Med.* **2020**, *8* (21), 1399.

(10) Bąk-Romaniszyn, L.; Świerzko, A. S.; Sokołowska, A.; Durko, Ł.; Mierzwa, G.; Szala-Poździej, A.; Małecka-Panas, E.; Cedzyński, M.

Mannose-Binding Lectin (MBL) in Adult Patients with Inflammatory Bowel Disease. *Immunobiology* **2020**, *225* (1), 151859.
(11) Fumagalli, S.; De Simoni, M. G. Lectin Complement Pathway and Its Bloody Interactions in Brain Ischemia. *Stroke* **2016**, *47* (12), 3067−3073.
(12) Neglia, L.; Fumagalli, S.; Orsini, F.; Zanetti, A.; Perego, C.; De Simoni, M. G. Mannose-Binding Lectin Has a Direct Deleterious Effect on Ischemic Brain Microvascular Endothelial Cells. *J. Cereb. Blood Flow Metab.* **2020**, *40* (8), 1608−1620.
(13) Ytting, H.; Christensen, I. J.; Thiel, S.; Jensenius, J. C.; Svendsen, M. N.; Nielsen, L.; Lottenburger, T.; Nielsen, H. J. Biological Variation in Circulating Levels of Mannan-Binding Lectin (MBL) and MBL-Associated Serine Protease-2 and the Influence of Age, Gender and Physical Exercise. *Scand. J. Immunol.* **2007**, *66* (4), 458−464.
(14) Dean, M.; Minchinton, R.; Heatley, S.; Eisen, D. Mannose Binding Lectin Acute Phase Activity in Patients with Severe Infection. *J. Clin. Immunol.* **2005**, *25* (4), 346−352.
(15) Garred, P.; Genster, N.; Pilely, K.; Bayarri-Olmos, R.; Rosbjerg, A.; Ma, Y. J.; Skjoedt, M. O. A Journey through the Lectin Pathway of Complement-MBL and Beyond. *Immunol. Rev.* **2016**, *274* (1), 74−97.
(16) Eisen, D. P.; Dean, M. M.; Boermeester, M. A.; Fidler, K. J.; Gordon, A. C.; Kronborg, G.; Kun, J. F. J.; Lau, Y. L.; Payeras, A.; Valdimarsson, H.; et al. Low Serum Mannose-Binding Lectin Level Increases the Risk of Death Due to Pneumococcal Infection. *Clin. Infect. Dis.* **2008**, *47* (4), 510−516.
(17) Auriti, C.; Prencipe, G.; Moriondo, M.; Bersani, I.; Bertaina, C.; Mondì, V.; Inglese, R. Mannose-Binding Lectin: Biologic Characteristics and Role in the Susceptibility to Infections and Ischemia-Reperfusion Related Injury in Critically Ill Neonates. *J. Immunol. Res.* **2017**, *2017*, 1−11.
(18) Sena, M.; da Silva Castanha, P.; Giles Guimarães, A.; Oliveira, P.; da Silva, M.; Cordeiro, M.; Moura, P.; Braga, C.; Vasconcelos, L. Mannose-Binding Lectin Levels and MBL2 Gene Polymorphisms Are Associated with Dengue Infection in Brazilian Children at the Early Ages. *Int. J. Infect. Dis.* **2022**, *117*, 212−219.
(19) De Pascale, G.; Cutuli, S. L.; Pennisi, M. A.; Antonelli, M. The Role of Mannose-Binding Lectin in Severe Sepsis and Septic Shock. *Mediators Inflamm.* **2013**, *2013*, 625803.
(20) Mrazkova, J.; Sistek, P.; Lochman, J.; Izakovicova Holla, L.; Danek, Z.; Borilova Linhartova, P. A SNaPshot Assay for Determination of the Mannose-Binding Lectin Gene Variants and an Algorithm for Calculation of Haplogenotype Combinations. *Diagnostics* **2021**, *11* (2), 301.
(21) Sunil Singh, S.; Chi Fai Cheung, R.; Ho Wong, J.; Bun Ng, T. Mannose Binding Lectin: A Potential Biomarker for Many Human Diseases. *Curr. Med. Chem.* **2016**, *23* (33), 3847−3860.
(22) Hosseini, S.; Vâzquez-Villegas, P.; Rito-Palomares, M.; Martínez-Chapa, S. O. Advantages, Disadvantages and Modifications of Conventional ELISA. *SpringerBr. Appl. Sci. Technol.* **2018**, 67115. .
(23) Chen, H.; Kou, X.; Yang, Z.; Ni, W.; Wang, J. Shape and Size-Dependent Refractive Index Sensitivity of Gold Nanoparticles. *Langmuir* **2008**, *24*, 5233−5237.
(24) Chen, H.; Shao, L.; Li, Q.; Wang, J. Gold Nanorods and Their Plasmonic Properties. *Chem. Soc. Rev.* **2013**, *42* (7), 2679−2724.
(25) Chang, H. H.; Murphy, C. J. Mini Gold Nanorods with Tunable Plasmonic Peaks beyond 1000 Nm. *Chem. Mater.* **2018**, *30* (4), 1427−1435.
(26) Cao, J.; Galbraith, E. K.; Sun, T.; Grattan, K. T. V. Sensors and Actuators B: Chemical Effective Surface Modification of Gold Nanorods for Localized Surface Plasmon Resonance-Based Biosensors. *Sens. Actuators B: chem.* **2012**, *169*, 360−367.
(27) Müller, C.; Despras, G.; Lindhorst, T. K. Organizing Multivalency in Carbohydrate Recognition. *Chem. Soc. Rev.* **2016**, *45* (11), 3275−3302.
(28) Baker, A. N.; Muguruza, A. R.; Richards, S. J.; Georgiou, P. G.; Goetz, S.; Walker, M.; Dedola, S.; Field, R. A.; Gibson, M. I. Lateral Flow Glyco-Assays for the Rapid and Low-Cost Detection of Lectins-Polymeric Linkers and Particle Engineering Are Essential for Selectivity and Performance. *Adv. Healthcare Mater.* **2022**, *11* (4), No. e2101784.
(29) Baker, A. N.; Richards, S. J.; Pandey, S.; Guy, C. S.; Ahmad, A.; Hasan, M.; Biggs, C. I.; Georgiou, P. G.; Zwetsloot, A. J.; Straube, A.; et al. Glycan-Based Flow-Through Device for the Detection of SARS-COV-2. *ACS Sens.* **2021**, *6* (10), 3696−3705.
(30) Georgiou, P. G.; Guy, C. S.; Hasan, M.; Ahmad, A.; Richards, S. J.; Baker, A. N.; Thakkar, N. V.; Walker, M.; Pandey, S.; Anderson, N. R.; et al. Plasmonic Detection of SARS-CoV-2 Spike Protein with Polymer-Stabilized Glycosylated Gold Nanorods. *ACS Macro Lett.* **2022**, *11* (3), 317−322.
(31) Erol, G.; Schmidt, P. P.; Pancaro, A.; Diaz, J. M. M.; Barrientos, A. G.; Porter, J.; Polito, L.; Szymonik, M.; Nelissen, I.; Spencer, D. I. R.; Piotti, A.; Beeg, M.; De Simoni, M.-G.; Fumagalli, S.; Gobbi, M. New Nanostructures Inhibiting Human Mannose Binding Lectin Identified by a Novel Surface Plasmon Resonance Assay. *Sens. Actuators B: Chem.* **2022**, *360*, 131661.
(32) Vonarbourg, A.; Passirani, C.; Saulnier, P.; Benoit, J. P. Parameters Influencing the Stealthiness of Colloidal Drug Delivery Systems. *Biomaterials* **2006**, *27* (24), 4356−4373.
(33) Suk, J. S.; Xu, Q.; Kim, N.; Hanes, J.; Ensign, L. M. PEGylation as a Strategy for Improving Nanoparticle-Based Drug and Gene Delivery. *Adv. Drug Deliv. Rev.* **2016**, *99*, 28−51.
(34) García, I.; Sánchez-Iglesias, A.; Henriksen-Lacey, M.; Grzelczak, M.; Penadés, S.; Liz-Marzan, L. M. Glycans as Biofunctional Ligands for Gold Nanorods: Stability and Targeting in Protein-Rich Media. *J. Am. Chem. Soc.* **2015**, *137* (10), 3686−3692.
(35) Zhao, Y.; Tong, L.; Li, Y.; Pan, H.; Zhang, W.; Guan, M.; Li, W.; Chen, Y.; Li, Q.; Li, Z.; et al. Lactose-Functionalized Gold Nanorods for Sensitive and Rapid Serological Diagnosis of Cancer. *ACS Appl. Mater. Interfaces* **2016**, *8* (9), 5813−5820.
(36) Barrientos, A. G.; De la Fuente, J. M.; Rojas, T. C.; Fernández, A.; Penadés, S. Gold Glyconanoparticles: Synthetic Polyvalent Ligands Mimicking Glycocalyx-like Surfaces as Tools for Glycobiological Studies. *Eur. J. Chem* **2003**, *9* (9), 1909−1921.
(37) Rajagopalan, R.; Salvi, V. P.; Jensenius, J. C.; Rawal, N. New Insights on the Structural/Functional Properties of Recombinant Human Mannan-Binding Lectin and Its Variants. *Immunol. Lett.* **2009**, *123* (2), 114−124.
(38) Leyva, A.; Quintana, A.; Sánchez, M.; Rodríguez, E. N.; Cremata, J.; Sánchez, J. C. Rapid and Sensitive Anthrone e Sulfuric Acid Assay in Microplate Format to Quantify Carbohydrate in Biopharmaceutical Products: Method Development and Validation. *Biologicals* **2008**, *36*, 134−141.
(39) Elst, K.; Babbar, N.; Van Roy, S.; Baldassarre, S.; Dejonghe, W.; Maesen, M.; Sforza, S. Continuous Production of Pectic Oligosaccharides from Sugar Beet Pulp in a Cross Flow Continuous Enzyme Membrane Reactor. *Bioprocess Biosyst. Eng.* **2018**, *41* (11), 1717−1729.
(40) Krpetić, Z.; Davidson, A. M.; Volk, M.; Lévy, R.; Brust, M.; Cooper, D. L. High-Resolution Sizing of Monolayer-Protected Gold Clusters by Differential Centrifugal Sedimentation. *ACS Nano.* **2013**, *7* (10), 8881−8890.
(41) Velimirovic, M.; Pancaro, A.; Mildner, R.; Georgiou, P. G.; Tirez, K.; Nelissen, I.; Johann, C.; Gibson, M. I.; Vanhaecke, F. Characterization of Gold Nanorods Conjugated with Synthetic Glycopolymers Using an Analytical Approach Based on SpICP-SFMS and EAF4-MALS. *Nanomaterials* **2021**, *11*, 2720.
(42) Liang, M.; Lin, I. C.; Whittaker, M. R.; Minchin, R. F.; Monteiro, M. J.; Toth, I. Cellular Uptake of Densely Packed Polymer Coatings on Gold Nanoparticles. *ACS Nano* **2010**, *4* (1), 403−413.
(43) Georgiou, P. G.; Baker, A. N.; Richards, S. J.; Laezza, A.; Gibson, M. I.; Walker, M.; Gibson, M. I. Tuning Aggregative versus Non-Aggregative Lectin Binding with Glycosylated Nanoparticles by the Nature of the Polymer Ligand. *J. Mater. Chem. B* **2019**, *8* (1), 136−145.
(44) Dheyab, M. A.; Aziz, A. A.; Moradi Khaniabadi, P.; Jameel, M. S.; Oladzadabbasabadi, N.; Mohammed, S. A.; Abdullah, R. S.; Mehrdel, B. Monodisperse Gold Nanoparticles: A Review on

https://doi.org/10.1021/acsami.4c04018
ACS Appl. Mater. Interfaces 2024, 16, 30556−30566

Synthesis and Their Application in Modern Medicine. *Int. J. Mol. Sci.* **2022**, *23* (13), 7400.
(45) Chang, J.; Zhang, A.; Huang, Z.; Chen, Y.; Zhang, Q.; Cui, D. Monodisperse Au@Ag Core-Shell Nanoprobes with Ultrasensitive SERS-Activity for Rapid Identification and Raman Imaging of Living Cancer Cells. *Talanta* **2019**, *198*, 45−54.
(46) Fuller, M.; Köper, I. Polyelectrolyte-Coated Gold Nanoparticles: The Effect of Salt and Polyelectrolyte Concentration on Colloidal Stability. *Polymers* **2018**, *10* (12), 1336.
(47) Pitirollo, O.; Micoli, F.; Necchi, F.; Mancini, F.; Carducci, M.; Adamo, R.; Evangelisti, C.; Morelli, L.; Polito, L.; Lay, L. Gold Nanoparticles Morphology Does Not Affect the Multivalent Presentation and Antibody Recognition of Group A Streptococcus Synthetic Oligorhamnans. *Bioorg. Chem.* **2020**, *99*, 103815.
(48) Strong, L.; Whitesides, G. M. Structures of Self-Assembled Monolayer Films of Organosulfur Compounds Adsorbed on Gold Single Crystals: Electron Diffraction Studies. *Langmuir* **1988**, *4* (3), 546−558.
(49) Schreiber, F. Structure and Growth of Self-Assembling Monolayers. *Prog. Surf. Sci.* **2000**, *65* (5), 151−257.
(50) Hinterwirth, H.; Kappel, S.; Waitz, T.; Prohaska, T.; Lindner, W.; Lämmerhofer, M. Quantifying Thiol Ligand Density of Self-Assembled Monolayers on Gold Nanoparticles by Inductively Coupled Plasma-Mass Spectrometry. *ACS Nano* **2013**, *7* (2), 1129−1136.
(51) Retout, M.; Brunetti, E.; Valkenier, H.; Bruylants, G. Limits of Thiol Chemistry Revealed by Quantitative Analysis of Mixed Layers of Thiolated-PEG Ligands Grafted onto Gold Nanoparticles. *J. Colloid Interface Sci.* **2019**, *557*, 807−815.
(52) Perez-Potti, A.; Lopez, H.; Pelaz, B.; Abdelmonem, A.; Soliman, M. G.; Schoen, I.; Kelly, P. M.; Dawson, K. A.; Parak, W. J.; Krpetic, Z.; et al. In Depth Characterisation of the Biomolecular Coronas of Polymer Coated Inorganic Nanoparticles with Differential Centrifugal Sedimentation. *Sci. Rep.* **2021**, *11* (1), 6443.
(53) Lara, S.; Alnasser, F.; Polo, E.; Garry, D.; Lo Giudice, M. C.; Hristov, D. R.; Rocks, L.; Salvati, A.; Yan, Y.; Dawson, K. A. Identification of Receptor Binding to the Biomolecular Corona of Nanoparticles. *ACS Nano* **2017**, *11* (2), 1884−1893.
(54) Francia, V.; Yang, K.; Deville, S.; Reker-Smit, C.; Nelissen, I.; Salvati, A. Corona Composition Can Affect the Mechanisms Cells Use to Internalize Nanoparticles. *ACS Nano* **2019**, *13* (10), 11107−11121.
(55) Heitzeneder, S.; Seidel, M.; Förster-Waldl, E.; Heitger, A. Mannan-Binding Lectin Deficiency Good News, Bad News, Doesn't Matter? *Clin. Immunol.* **2012**, *143* (1), 22−38.
(56) Gupta, A.; Gupta, G. S. Status of Mannose-Binding Lectin (MBL) and Complement System in COVID-19 Patients and Therapeutic Applications of Antiviral Plant MBLs. *Mol. Cell. Biochem.* **2021**, *476* (8), 2917−2942.
(57) Kawasaki, T. Structure and Biology of Mannan-Binding Protein, MBP, an Important Component of Innate Immunity. *Biochim. Biophys. Acta* **1999**, *1473* (1), 186−195.
(58) Pancaro, A.; Szymonik, M.; Georgiou, P. G.; Baker, A. N.; Walker, M.; Adriaensens, P.; Hendrix, J.; Gibson, M. I.; Nelissen, I. The Polymeric Glyco-Linker Controls the Signal Outputs for Plasmonic Gold Nanorod Biosensors Due to Biocorona Formation. *Nanoscale* **2021**, *13*, 10837−10848.
(59) Chen, W.; Zhong, Y.; Shu, J.; Yu, H.; Chen, Z.; Ren, X.; Hui, Z.; Li, Z. Characterization of Glucose-Binding Proteins Isolated from Health Volunteers and Human Type 2 Diabetes Mellitus Patients. *Proteins* **2021**, *89* (11), 1413−1424.
(60) Qiu, H.-Y.; Hou, N.-N.; Shi, J.-F.; Liu, Y.-P.; Kan, C.-X.; Han, F.; Sun, X.-D. Comprehensive overview of human serum albumin glycation in diabetes mellitus. *World J. Diabetes* **2021**, *12* (7), 1057−1069.
(61) Casals, E.; Pfaller, T.; Duschl, A.; Oostingh, G. J.; Puntes, V. Time Evolution of the Nanoparticle Protein Corona. *ACS Nano* **2010**, *4* (7), 3623−3632.
(62) Voltan, R.; Castaldello, A.; Brocca-Cofano, E.; Altavilla, G.; Caputo, A.; Laus, M.; Sparnacci, K.; Ensoli, B.; Spaccasassi, S.; Ballestri, M.; et al. Preparation and Characterization of Innovative Protein-Coated Poly(Methylmethacrylate) Core-Shell Nanoparticles for Vaccine Purposes. *Pharm. Res.* **2007**, *24* (10), 1870−1882.
(63) Monopoli, M.; Aberg, C.; Salvati, A.; Dawson, K. Biomolecular Coronas Provide the Biological Identity of Nanosized Materials. *Nat. Nanotechnol.* **2012**, *7* (12), 779−786.
(64) Jensen, P. H.; Weilguny, D.; Matthiesen, F.; McGuire, K. A.; Shi, L.; Højrup, P. Characterization of the Oligomer Structure of Recombinant Human Mannan-Binding Lectin. *J. Biol. Chem.* **2005**, *280* (12), 11043−11051.
(65) Teillet, F.; Dublet, B.; Andrieu, J. P.; Gaboriaud, C.; Arlaud, G. J.; Thielens, N. M. The Two Major Oligomeric Forms of Human Mannan-Binding Lectin: Chemical Characterization, Carbohydrate-Binding Properties, and Interaction with MBL-Associated Serine Proteases. *J. Immunol.* **2005**, *174* (5), 2870−2877.
(66) Kjaer, T. R.; Le, L. T. M.; Pedersen, J. S.; Sander, B.; Golas, M. M.; Jensenius, J. C.; Andersen, G. R.; Thiel, S. Structural Insights into the Initiating Complex of the Lectin Pathway of Complement Activation. *Structure* **2015**, *23* (2), 342−351.
(67) Vandooren, J.; Itoh, Y. Alpha-2-Macroglobulin in Inflammation, Immunity and Infections. *Front. Immunol.* **2021**, *12*, 803244.
(68) McMullen, M.; Hart, M.; Walsh, M.; Buras, J.; Takahashi, K.; Stahl, G. Mannose-Binding Lectin Binds IgM to Activate the Lectin Complement Pathway in Vitro and in Vivo. *Immunobiology* **2006**, *211* (10), 759−766.
(69) Ma, Y.; Doni, A.; Skjoedt, M.; Honoré, C.; Arendrup, M.; Mantovani, A.; Garred, P. Heterocomplexes Of Mannose-Binding Lectin And The Pentraxins PTX3 Or Serum Amyloid P Component Trigger Cross-Activation Of The Complement System. *J. Bio. Chem.* **2011**, *286* (5), 3405−3417.

https://doi.org/10.1021/acsami.4c04018
ACS Appl. Mater. Interfaces 2024, 16, 30556−30566